The Almighty Quasar — Destroyer of Worlds

Julia Ahlvind

Degree project C in Physics – Astronomy, 15 ECTS

Supervisor: Erik Zackrisson
Subject reader: Kjell Olofsson
Examiner: Matthias Weiszflog

Department of Physics and Astronomy
Uppsala University

June 12, 2019

UPPSALA
UNIVERSITET

Abstract

In the study of habitability of terrestrial exoplanets, both life-supporting conditions and the prevalence of transient life-threatening events need to be considered. One type of hazardous effect that has so far not received much attention is the thermal effect of a nearby active galactic nucleus (AGN), or in this particular case, the class of the AGN known as a quasar. In this work we investigate the thermal effect from a quasar by calculating the number of habitable terrestrial planets (HTP) in an elliptical or bulge-dominated galaxy, that goes extinct when exposed to the quasar radiation in a limited wavelength range. This is done by approximations and modelling along with pre-existing formulas and data from earlier publications. As a result, the influence by a quasar during the time span of quasar activity will have a less significant impact on the habitability in solar-type stellar systems than expected. Assuming $t_{QSO} = 10^8$ yrs of quasar activity, results in the number of affected HTP, $\approx 1 \times 10^5$, 9×10^5 and 4×10^8 for isotropic spherical radiation and $\approx 1 \times 10^6$, 8×10^6 and 3×10^9 for a double-conical radiation. In terms of stellar mass fraction, $\approx 1.3\%$, 1.0%, 0.4% for isotropic radiation and $\approx 12.8\%$, 9.5%, 3.8% for conical, is affected. The results of this work are hoped to provide a rough estimation of the thermal impacts of a quasar on the habitability as well as to point out the most important parameters when considering this model.

Sammanfattning

I studier om beboeligheten på jordlika exoplaneter övervägs både förutsätningar för liv på planeten men även livshotande händelser i planetens närhet. En typ av farlig effekt som hitintills inte fått mycket uppmärksamhet, är det termiska effekterna från en aktiv galaxkärna (AGN) eller som i detta fall, AGN-typen kvasar. I detta arbete studeras de termiska effekterna från en kvasar genom att beräkna antalet beboeliga jordlika exoplaneter (HTP) i en elliptisk eller bulge-dominerad galax, (bulge-centralförtätning), som blir obeboeliga då de utsätts för kvasarens strålning i ett begränsat våglängdsområde. Detta görs genom antaganden och modellering av redan befintliga formler och data från tidigare publikationer. Detta resulterar i en mindre inverkan av kvasaren på system kring sollika stjärnor än förväntat. Antaget $t_{QSO} = 10^8$ år av kvasar-aktivitet ger antal påverkade HTP, $\approx 1 \times 10^5$, 9×10^5 och 4×10^8 vid isotropisk strålning och 1×10^6, 8×10^6 och 3×10^9 vid dubbel-konisk formad strålning. Uttryckt i andel stjärnmassa motsvarar detta $\approx 1.3\%$, 1.0%, 0.4% för sfäriskt fall och $\approx 12.8\%$, 9.5%, 3.8% vid koniskt. Detta arbete hoppas kunna ge on grov uppfattning om kvasarens termiska effekter på beboligheten men även identifiera det mest betydande parametrarna i denna modell.

Contents

Chapter 1

Introduction

When searching for life in the universe, astronomers look for Earth-like planets with conditions favourable for life, i.e planets that are habitable. But the habitability of a planet is not the only aspect that needs consideration. Life-threatening events in the vicinity of a planet such as a supernova, an asteroid on a collision-course with the planet or a gamma-ray burst must also be taken into account. A less considered dangerous aspects is the thermal effects caused by a quasar. A quasar is a type of an active galactic nucleus (AGN), described as a mechanism driven by accretion onto a supermassive black hole (SMBH) thought to exist in the centre of all galaxies. The output by the accretion is in the form of a highly energetic electromagnetic radiation that extends far out in the afflicted galaxy.

The few existing studies in the field, such as the recent ones by Lingam et al. (2019), Forbes & Loeb (2018) & Balbi & Tombesi (2017), along with a few earlier ideas like Clarke (1981), suggest that the high energy radiation from such a stellar object could potentially have a lethal impact on the habitability on the near centre stellar systems in the host galaxy. By varying calculations and different models, they have found that at a distance, $\sim$pc up to $\sim$kpc from the SMBH, the planets becomes uninhabitable.

However, most of the present research in the field consider the radiation in the ultraviolet (UV) to X-ray ranges. These lead to the so-called ionization effects, which causes chemical changes and mass loss of the atmosphere of the exoplanet. The focus of this thesis is on the thermal effects, which means that the impacts by the AGN will be in a comparable way as the host star of a solar-type or i.e spectral type FGK. The wavelength-range of radiation from the quasar considered, will therefore be in the same span as for a solar type star, that causes water to vaporize on the surface and shifts the planet out of the circumstellar habitable zone (HZ). Both an isotropic-spherical and a double conical emission by the quasar is considered in this work to emphasise the dependence of the emission shape, where a conical emission would be caused by the dust-torus that prevents emission in the plane of accretion.

The host galaxies of the quasars considered are of an elliptical or bulge-dominated type. This means that the stars orbiting the SMBH are assumed to be moving in random orbits and are furthermore evenly distributed in all directions in comparison to a disk-shaped galaxy. Therefore when considering the stellar movement during the active time of the quasar, the galaxy type is of importance to the stellar mass affected. The dependence of galaxy type is likely more relevant in the case of conical emission—radiation in two opposite cones, perpendicular to the disk—since the movements of the stars is mostly within the disk itself. In an elliptical galaxy however, the movement of the stars are random which gives them a higher probability to pass thorough this conical region. The dependence will however be of importance for the spherical emission as well. Three different sizes of quasar host galaxies will be considered in the interest of a broader understanding and a more general result.

The goal for this project is to investigate the influence of a quasar on the habitability in bulge-dominated galaxies. The impact of thermal radiation from a quasar on the habitability of terrestrial exoplanets will be estimated through numerical calculations based on pre-existing equations for the HZs by Cuntz (2014). Along with models for the spectral energy distribution of quasars from Calistro Rivera et al. (2016) and together with black hole mass-luminosity relation used by Shankar et al. (2010) and of the black hole mass and the stellar mass of the surrounding galactic bulge from Häring & Rix (2004). Finally the number of habitable terrestrial exoplanets (HTP) around FGK-type stars will be assessed using a model from Zackrisson et al. (2016). By the described method, this thesis will provide an estimation of the number of habitable exoplanets orbiting a solar-type star, that at least some occasion in galactic history, has been exposed to potentially lethal radiation from an AGN in the home galaxy as well as to point out the most important parameters consider this model.

Chapter 2

Background

2.1 Quasars and AGNs

The main component and engine for an AGN is a SMBH, similar to a black hole but with masses in range of $M \approx 10^5$–$10^{10} M_\odot$ (King 2016). One theory of how it grows so massive is by Bondi accretion in their AGN phase (King & Pounds 2015), i.e it gravitationally attracts matter spherically from its host galaxy. Some of the matter spirals inward and falls past the event horizon—the radial distance from the black hole where the escape velocity is greater than the speed of light—and is added to the black hole. The remaining matter stays in orbit and forms a so-called accretion disk, where the particles rub against each other. This leads to frictional heating that illuminates the surrounding gas to high brightness. In fact it gets so bright that the luminosity can exceed a whole galaxy like the Milky Way (Forbes & Loeb 2018). The amount of light can vary at short timescales for an AGN, in some extreme cases hours up to decades. By measuring the brightness oscillation the size of the accretion disk can be extracted through relations between period and the speed of light. As the matter spiral inwards to the black hole, the angular momentum of the matter is transported out. The reduction in angular momentum means a loss in velocity, hence the matter falls to a lower orbit around the black hole. A closer orbit implies a release in orbital energy and therefore an increment in velocity. As the accretion continues the pressure rises and eventually forces the gas, now in form of relativistic particles to be pushed out along the magnetic field of the accretion disk, perpendicular towards the disk itself in form of relativistic radio-jets (Melott & Thomas 2011).

The luminosity is one of the critical parts in classifying the AGN as a quasar, since there are other objects related to the AGN. In 1993, a unification theory for the AGNs was suggested by Antonucci (1993). The theory proposed a model for where the different objects such as quasars, blazars, Seyfert galaxies and radio galaxies are all the same phenomena viewed from different perspectives, see figure (2.1). All of the objects are thought to have accretion on to a SMBH and a surrounding dust torus in the centre of the galaxy, but when comparing their spectra, some things distinguish them from each other. If the orientation relative to the line of sight is such that the observation of the AGN is in the same plane as the torus and accretion disk, the short-wave radiation from the accretion will be absorbed by the torus, leaving the less energetic longer wavelengths such as infrared (IR) radiation, to propagate. The spectrum does not have broad emission lines since the fast-moving gas in the accretion is not observable. We call this a Radio or possibly Seyfert 2 galaxy. When viewing the AGN perpendicular to the disk and directly into the eye of the jet, the object is referred to as a blazar. These show emission lines in most wavelengths from X-rays to radio and are very luminous. The remaining classification is quasar (or Seyfert type 1). Their spectra show broad emission lines since we are observing the fast-moving matter in the accretion disk by viewing the AGN from a side way, in between the jet-beam and in the

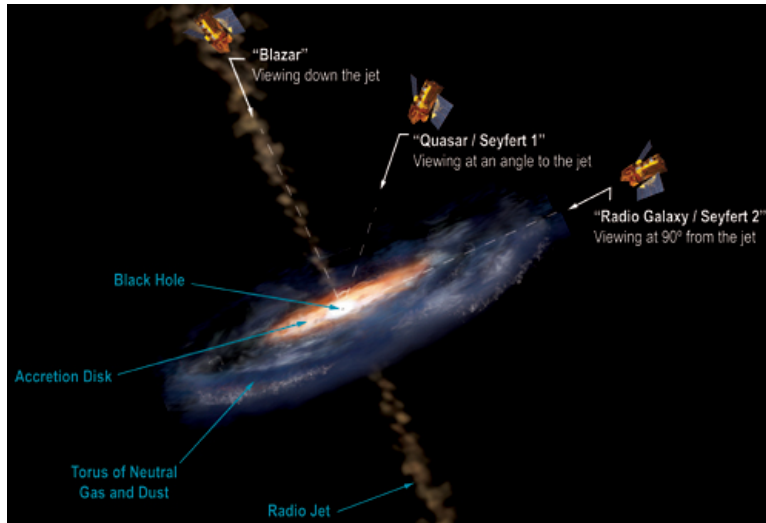plane of the torus. These are the most luminous out of all AGN- types and the one used in this thesis.

Figure 2.1: *The figure shows an illustration of the unification theory as well as the main components of an AGN. (Image credit: Aurore Simonnet, Sonoma State University, licenced under under CC BY 2.0.)*

2.1.1 Eddington limit

The timescale for which the quasar is active is called the duty cycle. That is when the quasar is emitting radiation at a high rate, giving them high luminosity and the interval for when it is affecting the habitability of a planet. At some stage in the duty cycle where the quasar is in hydrostatic equilibrium, meaning that the radiation pressure outward is equivalent to the gravitational force inward, the accretion will reach maximum bolometric luminosity, the Eddington limit. This is a theoretical limit where all energy produced in the process is emitted outward as luminous radiation. Though this maximum bolometric luminosity is an upper limit, it is not necessarily achieved since some of the energy may fall beyond the event horizon and gets accumulated by the black hole. The attained bolometric Eddington luminosity in a common accretion is around 10% of theoretical maximum and is also the value that will be used later on in the calculations.

The duty cycle is estimated by several relations between the black hole and bolometric luminosity. The luminosity of a quasar during the active phase is among other things, depending on the mass of the black hole. Such a relation was derived by Shankar et al. (2010) and is given as:

$$L_{Edd} = 1.26 * 10^{38} erg s^{-1} (\frac{M_{BH}}{M_{\odot}})$$ (2.1)

Where the mass of the black hole M_{BH} is expressed in solar masses, $M_{\odot}$ and the result, the Eddington luminosity L_{edd} in [erg s^{-1}]. The black hole mass can then in turn be related to the stellar mass of the surrounding bulge or stellar mass of the whole galaxy in case of an elliptical or irregular galaxy, where a more massive bulge will provide a higher bolometric luminosity. This bulge-BH mass relation was derived by Häring & Rix (2004) based on a linear regression from an earlier work by Akritas & Bershady (1996) and is shown in eqn. (2.2). Both black hole mass, M_{BH} and bulge mass, M_{bulge} is expressed in solar masses.

$$log(\frac{M_{BH}}{M_{\odot}}) = (8.20 \pm 0.10) + (1.12 \pm 0.06) log(\frac{M_{bulge}}{10^{11} M_{\odot}})$$ (2.2)

2.2 Definition of habitability

There are several ways to define the habitable zone. In search of extraterrestrial life we look for conditions that support biological life as we know it here on Earth. But conditions that differ from our home planet does not necessarily imply that we need to rule out the possibility that the exoplanet host life, nor does it mean that a planet inside the HZ necessarily must provide it. The definition that will be used in this report for the HZ is the same as the one used by Kasting et al. (2014) and Gale & Wandel (2017), where they define the HZ as a region around a star where planets inside have a surface temperature and atmosphere favourable for liquid water on, at least parts of its surface. In previous work by Kasting et al. (1993), the HZ is defined in two ways. The conservative habitable zone (CHZ) and the generalized habitable zone (GHZ). Where the inner limit of the CHZ is determined by the occurrence of water loss by hydrogen escape into space and the outer limit by the formation of CO_2 clouds at a temperature around 237K. The GHZ is limited by the greenhouse effect (see section 2.2.1). The calculations in this thesis will be based on previous work from Cuntz (2014) of HZs for planets orbiting a single star, with the conditions of GHZ, same as the ones used by Selsis et al. (2007).

2.2.1 Greenhouse effect

For an estimation of the GHZ around a star we have to take into account several parameters that could affect the conditions required to sustain liquid water on the surface. One of these parameters is the atmosphere of the planet. The earth atmosphere has a big optical depth at most infrared wavelengths, which generates a greenhouse effect that in turn heats the planet. A thicker atmosphere increases the temperature since it prevents the thermal radiation to escape and lack of one lowers it drastically. Therefore planets with a thicker atmosphere will be able to sustain liquid water on its surface further out from the host star. The greenhouse effect will therefore be important for the limits of the GHZ, wherein the calculation the same approach as Kasting et al. (1993) will be used. An estimate of the inner limit of the HZ is then determined by the runaway greenhouse effect and the outer one by the maximum greenhouse effect. The runaway greenhouse effect is described as the event when the temperature of the planet's surface exceeds the limit for where the water can be kept liquid. It can also be represented as the condition where the incoming stellar radiation overruns the outgoing thermal-IR radiation, but the both definitions are in practice the same since the last-mentioned also result in an increased surface temperature. The maximum greenhouse effect is explained as when the warming by CO_2 is at maximum. That means that the stellar flux can barely keep the surface temperature at 273K and the increasing albedo—the reflecting ability of radiation of the planet–makes the absorption of thermal radiation even less (Kasting et al. 2014).

In relation to this we need to consider the different spectral types of stars due to their varying radiation amount and wavelength. The incoming stellar flux from a star such as our own (G2 type in *Harvard Spectral Classification*) is higher compared to a small, cooler M-dwarf. For a star as M-dwarf or "Red Dwarf Star" (K-M spectral type), the HZ is considered to be located closer to the star (Gale & Wandel 2017). In this thesis the host star of the systems with orbiting HTPs are of solar-type or i.e FGK-stars with effective temperature in the range of $\sim 3900 - 7600K$ (Habets & Heintze 1981).

2.3   Radiation effects

The electromagnetic radiation emitted from a quasar could affect the habitability of a HTP in several ways. These can be divided into two main categories–indirect and direct. Where the indirect ones can be e.g ionization effects, leading to chemical changes in the planetary atmosphere, causing destruction of the ozone layer and making the radiation of the host star dangerous (Melott & Thomas 2011). The focus in this thesis however, lies on the direct–thermal effects. Suggesting that the radiation from the quasar has the same impact as the radiation from the star in the system, or i.e radiates at the same level, exposing the planet to more radiation that will increase the temperature causing the water on the surface to vaporise and with that shift the planet out of the original HZ.

In this thesis, we consider radiation from a restricted range in wavelengths, 1000-40 000 Å. This particular region is chosen due to atmospheric models, i.e the general range of wavelengths emitted from the Sun that is considered in models of the Earth's atmosphere. Different molecules in the atmosphere are responsible for absorbing the radiation in corresponding ranges of wavelength. Some of those molecules are ozone (O_3), that absorbs much of the shorter wavelengths in the visible range to ultraviolet (UV) $\leqslant 0.35$ μm & 0.5-0.7 μm, carbon dioxide (O_2), that works near the infrared (IR) in the visible part of spectra, around 0.7 μm and finally the biggest absorber, water (H_2O), that absorbs the long-waved radiation in the IR range 0.7-4 μm (Lacis & Hansen 1974). Water is therefore not only essential for life in liquid form on the surface of the planet but also as protection from radiation in the atmosphere.

2.4   Galaxies

The radiation effects from a quasar will look different depending on where in the galaxy, and in what type of galaxy that is considered. In 1926 *Edwin Hubble* invented the *Hubble sequence*, which is a classification scheme for galaxies. There the galaxies are divided into three main groups, namely ellipticals, spirals, lenticulars and an additional one, irregular. In this section, the difference between these galaxies and its impact on the quasar radiation is discussed.

2.4.1   Spiral galaxies

All spiral galaxies like the Milky Way, is thought to have a supermassive black hole in its center, surrounded by a rotating disk of gas, dust and stars—not to be confused by the accretion disk of an AGN. The movement of the stars in the disk are regular and in most cases follows a circular orbit around the centre of the galaxy. Here is also where most of the star formation takes place due to a higher concentration of gas and dust. The central part of the galaxy, outside the SMBH is known as the bulge, where a higher concentration of stars exists and share properties to an elliptical galaxy. The stars move in a random ways in the bulge, not following any particular orbital path in a disk but rather elliptical orbits inside a spheroid. The bulge consists primarily of population I stars—younger stars with high metallicity. Finally surrounding the disk and the central bulge do the stellar halo. Out here lies the globular clusters that are strong gravitationally bound spherical collections of older stars.

The impact from a quasar in this type of galaxy would differ from the case of e.g an elliptical galaxy. The stellar mass density is generally lower in a disk compared to in a bulge. This means that a uniformly spread radiation will affect less stellar mass within the disk compared to within the bulge. The direction of the jet-emission is more likely to be directed close to the perpendicular axis of the accretion disk, but due to the thickness of the disk, the jet also encounters the stars within it.

2.4.2 Elliptical galaxies

These type of galaxy are structureless compared to a spiral one, but share the property of having a SMBH in its centre. As previously mentioned they share properties to the bulge and therefore in the vicinity of an AGN, the radiation effects caused by a quasar will appear similar. These galaxies are mostly built up by low-mass stars since the high-mass ones have burnt out and have not been replaced by newer, due to a low star-formation rate. The distribution of stars in an elliptical galaxy or bulge is such that the highest concentration of stars is placed in the central parts, at the closest distance to the SMBH and decreasing exponentially when moving outwards. This implies that a higher fraction of stars will be affected by the AGN closer to the centre. These types of galaxies are the ones that will be used in the calculations and models later on alike Stanway et al. (2018) due to their simpler structure.

2.4.3 Lenticular galaxies

Lenticular galaxies are an intermediate type between spiral and elliptical galaxies according to Hubble's classification. Like the spiral galaxies they also have compounds such as a disk and a spherical shaped bulge in its centre parts. However, the lenticular ones do not have distinguishable spiral arms. The common feature with elliptical galaxies is the minimal interstellar medium which means they also have a low fraction of star formation and the stars that do exist are of the same type as the one found in elliptical galaxies.

2.4.4 Irregular galaxies

The remaining galaxies that do not fall into the previous three categories are part of the irregular galaxy classification. They lack the presence of any nuclear bulge or disk. They are thought to be formed in the presence of a large gravitational force, for instance a merger of two galaxies of the other classes.

Chapter 3

Modeling

In order to estimate how big impact the quasar thermal radiation could have on the habitability throughout a galaxy, the following approach is made and evaluated.

3.1   Quasar kill-radius

The limit up to where the accretion radiation is said to be destructive for a habitable terrestrial planet—the quasar kill-radius—is obtained by first assuming that an AGN emits radiation in the same way as a star, namely by black body radiation. Therefore one can make use of the formulas derived by Selsis et al. (2007), that estimates the limits of the habitable zone around a star and equate the inner limit of the HZ of the quasar ($d_{in} = d_{kill}$) with the kill-radius. The formulas used in the paper by Selsis is given as:

$$d_{in} = (d_{in\odot} - a_{in}T_\star - b_{in}T_\star^2)\sqrt{\frac{L}{L_\odot}}, \ [AU] \tag{3.1}$$

$$d_{out} = (d_{out\odot} - a_{out}T_\star - b_{out}T_\star^2)\sqrt{\frac{L}{L_\odot}}, \ [AU] \tag{3.2}$$

Where $d_{in\odot/out\odot}$ is the limits of the HZ of the solar system, measured in astronomical units (AU) and differs in value depending on the definition of habitability. The one adopted here is, as previously stated the one defined by GHZ namely, $d_{in\odot} = 0.84$ which corresponds to the distance from sun where the runaway greenhouse effect with no clouds starts and $d_{out\odot} = 1.67$ that sets the distance from the sun where the maximum greenhouse effect is achieved without cloud formation. The luminosity adopted here is the luminosity in the restricted wavelength-range of interest that is discussed in later sections. The scalars a and b is determined by regression and estimated to $a_{in} = 2.7619 \times 10^{-5}$, $b_{in} = 3.8095 \times 10^{-9}$ in the same paper by Selsis. The temperature $T_\star$ is measured in Kelvin(K) and is defined as $T_{eff} - 5700$, the effective temperature of the star minus a rough estimate of the effective temperature of the sun. The effective temperatures that are used are the temperature of FGK-stars as mentioned in section 2.2.1. The inner limit gives then the theoretical value of the quasar kill-radius for an isotropic radiating—spherically symmetric emission—of the AGN like a star.

As a rough estimation of the kill-radius and for a consistency check, the distance is also calculated by the non temperature-dependent relation:

$$d_{kill,rough} = \sqrt{\frac{L}{L_\odot}}/206265 \tag{3.3}$$

From the formula of brightness, F, and comparison to the sun, where we know the inner limit of the solar systems HZ, i.e the kill-radius of the sun, we can derive the kill-radius of

the quasar. To keep the brightness constant as it is observed from the Earth when replacing the source from the Sun to a quasar, the distance needs to be increased. The new derived distance is then the quasar kill-radius.

$$F = \frac{L}{4\pi d_{kill}^2} = \frac{L_\odot}{4\pi D_{AU}^2} \qquad (3.4)$$

Where L is the bolometric luminosity of the quasar, $L_\odot$ is the solar luminosity and D_{AU} is the distance between the Earth and the Sun, here measured in pc (D_{AU}=1/206265).

3.2   Template spectrum

A common way to display the quasar luminosity is by a so-called template spectrum or a spectral energy distribution (SED), where the luminosity is graphed as a function of wavelength or frequency. Such a spectrum is shown in figure (3.1) where the graph is based on data from Elvis et al. (2012). Integration is applied over the whole spectrum to obtain the total bolometric luminosity as well as over the restrained frequency span for the limited range which is marked in red in the same figure, (1000-40 000 Å). The ratio, R of the restricted and bolometric luminosity is obtained and later used to scale the attained bolometric luminosity from mass-relations described in the next section.
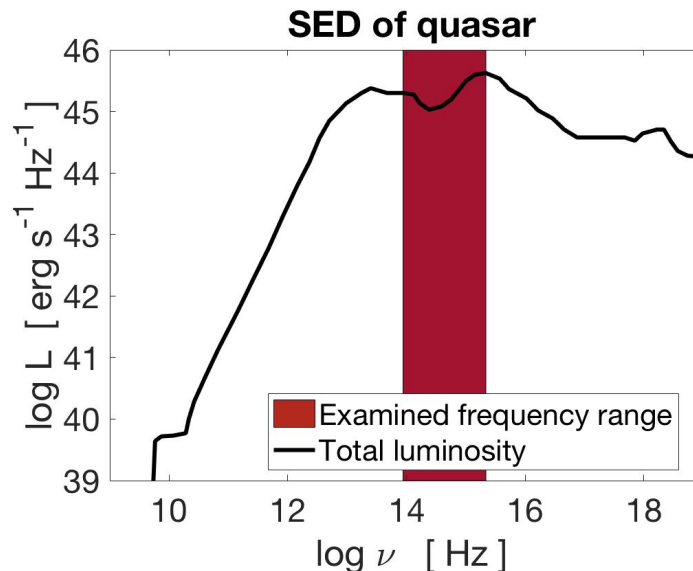

Figure 3.1: *The figure shows a mean spectral energy distribution of quasars in the logarithmic scale with the examined range of wavelength marked in red.*

3.3   Mass-luminosity relation

As previously stated, there is a close relation between the bulge mass and the black hole mass given in eqn. (2.2). This is a linear relation and can be plotted to demonstrate it as in figure (3.2), where the black line is a linear fit and the marked stars are the bulge masses used in this thesis.

By rewriting the eqn. (2.2), the expression for the black hole mass as a function of bulge mass is achieved:

$$\frac{M_{BH}}{M_\odot} = 10^{(8.20\pm0.10)+(1.12\pm0.06)log\left(\frac{M_{bulge}}{10^{11}M_\odot}\right)} \qquad (3.5)$$

The obtained black hole mass is then used in eqn. (2.1), to calculate the corresponding Eddington luminosity. Henceforth the bolometric luminosity is achieved through the estimation, aforementioned to be 10% of the Eddington luminosity.

Thereafter the attained bolometric luminosity is multiplied by the previously calculated luminosity ratio to get the quasar luminosity in the wanted wavelength span that corresponds to the regarding bulge mass:
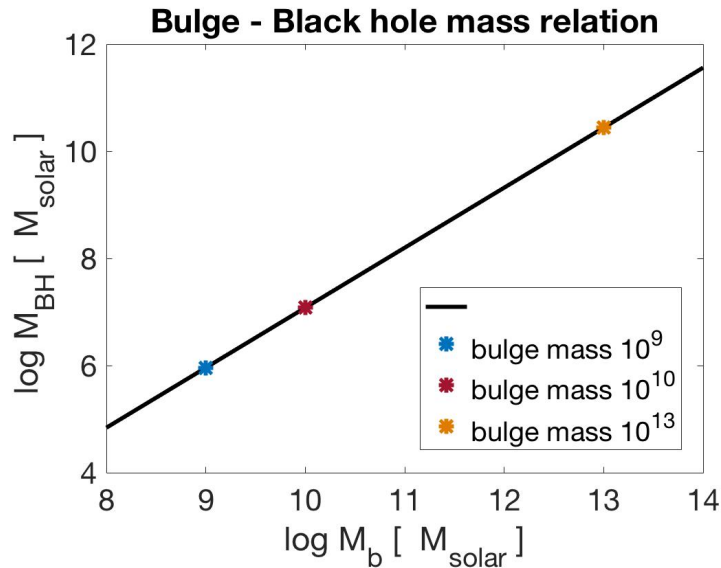
$$R \times L_{bol} = L \tag{3.6}$$

Figure 3.2: *The figure shows the logarithmic scale of the relation between bulge mass and black hole mass as a black line and three specific bulge masses marked as stars.*

Three bulge masses are marked in figure (3.2). These correspond to typical values of a smaller elliptical galaxy, able to host a SMBH, a commonly sized bulge-dominated galaxy as well as a massive—upper mass-limit—elliptical galaxy.

3.4 Stellar distribution

The stellar density in a bulge or in an elliptical galaxy is decreasing with distance from centre. This means that more stars will be affected in the closer regions of the SMBH. In the proceeding calculations for the stellar density, a model created by Plummer (1911) is used.

$$\rho(r) = \frac{3M_b}{4\pi} \frac{a^2}{(a^2 + r^2)^{5/2}} \tag{3.7}$$

Where M_b is the stellar bulge mass measured in solar-mass units, r is the corresponding kill-radius for the bulge mass concerned, in parsec (pc). The parameter a is the *Plummer radius*, which is a scale parameter approximated to be equivalent to the cluster core radius—the distance beyond which the stellar density drops significantly—also measured in pc. Therefore a is determined for each bulge size by a formula for the cluster core radius from the book by Meier (2012) and is presented in eqn. (3.8).

$$a = r_c = 48pc \left(\frac{M_{bulge}}{10^{10} M_{\odot}} \right)^{1/2} \tag{3.8}$$

10

The stellar mass enclosed by the kill-radius could then be obtained by integration of the density times the volume element, up to the limits of the sphere with radius equal to the kill-radius:

$$M_{sphere} = \int_0^{2\pi} \int_0^{\pi} \int_0^{d_{kill}} \rho(r)r^2 sin(\phi)d\varphi d\phi dr \qquad (3.9)$$

3.5 Radiation through jet vs isotropic

In the following step the form of emission is considered, i.e not spherically symmetric radiation from the quasar core but rather in two cone-shaped symmetric opposite jet-beams, or more precisely, two spherical sectors. The change in luminosity for jets is derived using a relation of the solid angle for the two cases. The solid angle for the jet is given as:

$$\Omega_{jet} = 2\pi(1 - cos(\theta/2)) \qquad (3.10)$$

Where θ is the two-dimensional opening angle of the quasar set to a mean value of the most common opening angles of radio-jet from (Pushkarev et al. 2011), $\theta = 15°$. And $\Omega_s = 4\pi$ for the sphere. The ratio, R_{angle} between the solid angles gives a numerical factor of luminosity increment for the two jet-beams.

$$R_{angle} = \frac{\Omega_s}{2\Omega_{jet}} = \frac{4\pi}{2 \times 2\pi(1 - cos(\theta/2))} \qquad (3.11)$$

$$L_{jet} = R_{angle} \times L \qquad (3.12)$$

This is then used as a scaling factor to scale the luminosity to the conical case as in eqn. (3.12) so that previous calculations involving luminosity can be re-evaluated for the conical emission, for example the kill-radius in eqn. (3.1). When calculating the enclosed stellar mass for jet-beams a similar integration as eqn. (3.9) is used, but with a smaller limiting angle φ.

$$M_{jet} = \int_0^{2\pi} \int_0^{\theta/2} \int_0^{d_{kill}} \rho(r)r^2 sin(\phi)d\varphi d\phi dr \qquad (3.13)$$

The jet-beams are approximated to a similar form as the radio-jets of a quasar and along with the assumption that all of the radiation would be pushed out through these jets. This would provide an extreme case situation i.e an exaggerated upper limit since in reality, not all luminosity propagate through these cones. If it did, we would not be able to observe parts of the AGN such as the accretion disk and torus, nor observe the opening angle itself.

3.6 Stellar movement

Since the quasar is active during a long period of time, $t_{QSO} \approx 10^6 - 10^8$ yrs according to Martini (2004), stars move inside the cluster and can pass through the jet. This means that more then the instant enclosed stellar mass will be affected. In order to estimate the stellar movement the $M - \sigma$ relation, eqn. (3.14) from Meier (2012) is used.

$$\sigma_{v,3D} = 108 km s^{-1} \left(\frac{M_{bulge}}{10^{10} M_\odot} \right)^{1/4} \qquad (3.14)$$

Where the $\sigma_{v,3D}$ is the three-dimensional velocity dispersion–dispersion of the mean velocity of the stars. This velocity is converted into one-dimensional velocity, $\sigma_{v,1D}$ by a scaling factor $1/\sqrt{3}$ according to Munari et al. (2013), in order to be used in the following step.

$$\sigma_{v,1D} = \frac{\sigma_{v,3D}}{\sqrt{3}} \qquad (3.15)$$

The stars are assumed to move in a random way throughout the bulge and at some time pass through the volume of radiation. The calculations proceed by the use off the mass flow rate (MFR), meaning that when stars are intersecting the jet, they are assumed to approach a conical cross-section from different directions with distribution ρ according to eqn. (3.7) and with velocity according to eqn. (3.15). The MFR is then obtained by integration of the density times stellar velocity and area element:

$$MFR_{jet} = \int_0^\theta \int_0^{d_{kill,jet}} \rho \sigma_{v,1D} r d\phi dr \qquad (3.16)$$

The total stellar mass passing through the cross-section can then be evaluated according to eqn. (3.17)

$$M_{tot,jet} = MFR_{jet} \times t_{QSO} \qquad (3.17)$$

In comparison to the conical emission, the total mass affected over time is also calculated for spherical emission case, where the same method is used but instead of the cross-section of a cone a circular one is used, meaning that the integration becomes:

$$MFR_{sphere} = \int_0^{2\pi} \int_0^{d_{kill,sphere}} \rho \sigma_{v,1D} r d\phi dr \qquad (3.18)$$

Where the spherical kill-radius, $d_{kill,s}$ is calculated according to eqn. (3.1) with initial derived luminosity L by eqn. (3.6) and not the jet-luminosity. The total stellar mass affected over t_{QSO} with spherical emission is then:

$$M_{tot,sphere} = MFR_{sphere} \times t_{QSO} \qquad (3.19)$$

3.7 Exoplanets

To asses the number of HTPs affected by the QSO radiation we first calculate the number of stellar systems around FGK-stars with orbiting terrestrial planets (TP), by multiplying the total stellar mass evaluated in the previous step by the factor $N_{FGK,TP} = 0.035$, which gives the the number of TPs per stellar mass. Thereafter the number of initially habitable planets, HTP is calculated by multiplying with $N_{HTP} = 1/4$. Where both factors are taken from Zackrisson et al. (2016).

$$N = M_{tot} \times N_{FGK,TP} \times N_{HTP} \qquad (3.20)$$

M_{tot} is the total mass affected by QSO radiation measured in solar mass unit.

Chapter 4

Result and analysis

For the given galaxies with stellar bulge mass $m_b = 10^9$ $M_\odot$, 10^{10} $M_\odot$ and 10^{13} $M_\odot$, the related core radius is derived to $r_c \approx 15$ pc, 48 pc, 1518 pc and the half-mass radius $r_{1/2} \approx$ 20 pc, 63 pc and 1981 pc. The number of affected HTPs in the various galaxy sizes was estimated to $N_{sphere} \approx 1 \times 10^5$, 9×10^5 and 4×10^8 for spherical radiation and $N_{jet} \approx 1 \times 10^6$, 8×10^6 and 3×10^9 for jet-emission. In terms of stellar mass fraction $\approx 1.3\%$, 1.0% and 0.4% is obtained for isotropic emission and $\approx 12.8\%$, 9.5% and 3.8% for jet-emission. Each with a corresponding kill-radius: for spherical situation $d_{kill,sphere} \approx 0.1$ pc, 0.5 pc, 22.9 pc, and $d_{kill,jet} \approx 1.4$ pc, 5.2 pc, 247.4 pc for jet-emission. The rough estimation of kill-radius for spherical emission of bolometric luminosity according to eqn. (3.3) were estimated to $d_{kill,rough} \approx 0.3$ pc, 1.0 pc and 46.2 pc.

Here on in this chapter, some of the result and their significance will be evaluated.

4.1 Temperature independence

In the given formula for the limits of the habitable zone, there is not only dependence on the stellar luminosity but also of the effective temperature. This temperature dependence is according to Selsis et al. (2007), caused by the relation between the effective temperature of the host star and the albedo of the orbiting planet. In the article they also state that the albedo changes because of the relay scattering which is increased in the infrared ranges due to absorption by water and carbon dioxide, as the spectral range of the star shifts to that area. Another explanation of the temperature dependence is that a lower effective temperature gives rise to a greater infrared fraction in the luminosity as a result of the shift in the black body curve. The bigger the fraction, the larger the greenhouse effect will be. This means that the limits of the HZ is closer to the star than it would be if the temperature did not have any effect.

However in the range of this thesis the effects by the difference in temperature for FGK stars on the HZ is negligible. The distance variation of the HZ, or in our case the quasar kill-radius, is small and have a negligible impact on the number of HTP affected. The temperature dependence is shown in figure (4.1) where the HZ limits are based on a solar-type star with solar-luminosity. Calculations were therefore based on a solar-type temperature of $T_{eff} = 5800$ K.
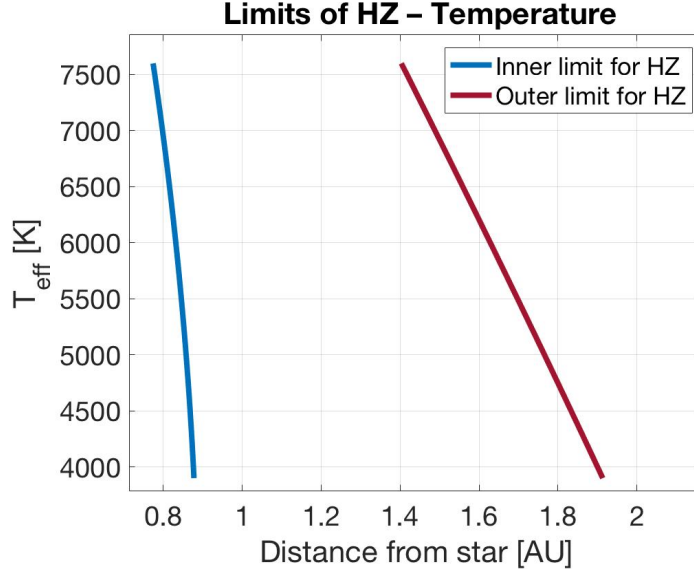
Figure 4.1: *The figure shows the limits of the habitable zone as a function of temperature for FGK-stars with solar luminosity.*

4.2 Spherical vs conical

For the galaxies with three different stellar mass used in this thesis, the spherical luminosity of the AGN in the restricted wavelength range was calculated to: $\log_{10} L_{sphere} \approx 42$ erg s^{-1}, 44 erg s^{-1}, 47 erg s^{-1} in comparison to where all luminosity is said to be directed into two jet-beams, $\log_{10} L_{jet} \approx 45$ erg s^{-1}, 46 erg s^{-1}, 49 erg s^{-1}. This luminosity increment for the situation with two jets is clearly something that affects the range of the kill-radius based on eqn. (3.1). Calculating the corresponding kill-radius for the two cases gives a result of $d_{kill,sphere} \approx 0.1$ pc, 0.5 pc, 22.9 pc for the isotropic radiation and $d_{kill,jet} \approx 1.4$ pc, 5.2 pc, 247.4 pc in the event of two jets as previously stated. Again, one needs to point out that this is a "worst case scenario" since not all of the luminosity generated in the accretion goes out in these two jets. The general relation for each situation between bulge mass and kill-radius is shown in figure (4.2), where it is clear that the kill-radius always reaches further out in the galaxy for the jet-emission. In the same figure, the rough estimated kill-radius by eqn. (3.3) dependent on the bolometric luminosity, is also shown. It indicates that, despite the limited frequency range, the jet-emission gives a longer kill-radius and the isotropic emission, a shorter. However, it shows that the two ways of calculating are somewhat consistent with each other.

When deriving the momentarily stellar mass affected by the quasar, i.e the enclosed stellar mass of the kill-radius for isotropic and conical radiation, the result is as follows. For spherical radiation the instantaneously enclosed stellar mass is, $M_{sphere} \approx 7 \times 10^2$ $M_\odot$, 1×10^4 $M_\odot$, 3×10^7 $M_\odot$ for respectively galaxy size. Whereas for jet case, $M_{jet} \approx 7 \times 10^3$ $M_\odot$, 1×10^5 $M_\odot$, 4×10^8 $M_\odot$. It is clear that the increment in kill-radius has a large impact on the amount of affected stellar mass since the enclosed mass is less in the spherical situation compared to the conical one despite the reduced solid angle. Even so, the increment in kill-radius for jet case generates a larger "kill-conical volume" than "kill-spherical volume".
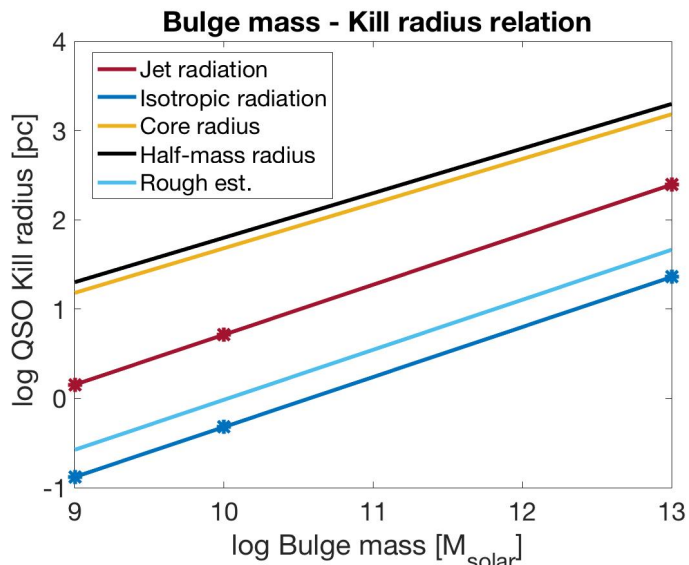
Figure 4.2: *The figure shows the logarithmic relation between bulge mass and the QSO kill-radius for isotropic and two jet-beam emission as well as for the rough estimated kill-radius from the equation of brightness. It also shows the linear relation for the core radius and the half-mass radius.*

4.3 Momentarily vs over time

By comparing the momentarily affected stellar mass to the one affected during the time of quasar activity, is it clear that the time is an important parameter when considering this model. The stellar mass exposed to QSO radiation instantaneously–the mass enclosed by the cone defined by the opening angle and kill-radius is, $M_{jet} \approx 7 \times 10^3 \ M_\odot, \ 1 \times 10^5 \ M_\odot, \ 4 \times 10^8 \ M_\odot$. and the stellar mass affected over time–passing through conical cross-section during the active time of QSO, $M_{tot,jet} \approx 1 \times 10^8 \ M_\odot, 9 \times 10^8 \ M_\odot$ and $4 \times 10^{11} \ M_\odot$. A similar result is obtained for the spherical case, $M_{sphere} \approx 7 \times 10^2 \ M_\odot, \ 1 \times 10^4 \ M_\odot, \ 3 \times 10^7 \ M_\odot$ and over time, $M_{tot,sphere} \approx 1 \times 10^7 \ M_\odot, \ 1 \times 10^8 \ M_\odot, \ 4 \times 10^{10} \ M_\odot$.

Worth to point out is that the movements are not based on a completely realistic case as mentioned earlier, since stars do not move on a one dimensional string towards the cone or sphere of lethal radiation, but rather in random elliptical orbits. For a more accurate estimation, an n-body simulation could be used to get more realistic movements and amount of stellar mass passed through it, which is unfortunately outside the scope of this thesis. In any case this implies that the total stellar mass affected is an upper limit and is most likely lower in reality. Nevertheless is it obvious that time and stellar movement is important parameters that should not be neglected when estimating the thermal effects of an AGN.

The stellar movement as previously stated, differs between the galaxy types. Therefore when comparing quasar impact momentarily and over time, it changes between the different types. In an elliptical galaxy the stars move in random orbits around the SMBH. The impact is therefore equal regardless of the direction of the emission. In a disk-shaped galaxy without bulge however, the impact is not equally distributed. Since the majority of the matter such as dust and stellar systems is located in the disk, the quasar radiation will spread further out perpendicular to the disk but also affect less stellar mass. The radiation in the direction closer to the accretion plane will therefore affect more stellar mass, which would then probably give us a larger impact from the quasar in the case of spherical emission, even though the jet-emission also affects some of the stellar mass within the disk. Comparing the result to an elliptical or bulge-dominated galaxy will not only differ due to these mentioned

factors, but also because of the different stellar mass density. The density within the disk is generally lower than in a bulge, as mentioned earlier, thus the same quasar kill-volume gives a lower affected mass in the disk. Therefore the spherical and jet-emission case considered in this thesis would in a disk-shaped galaxy be significantly more complicated to derive and in the end give us a different result.

Chapter 5

Improvements and future prospects

In this thesis there are, as previously mentioned, assumptions and neglected parameters that would affect the result of the impact from an AGN on the habitability of HTPs. Some of those parameters will be discussed in this section.

5.1 Quasar and black-body radiation

The assumption that a quasar would emit radiation like a black body is not true. However, in the range of this thesis we consider it to be a valid assumption based on fitting-models of AGNs (Calistro Rivera et al. 2016). A SED of a quasar extends over the full range of the electromagnetic spectrum between radio waves to X-rays and has in contrast to the black body spectrum, several bumps (see figure (3.1)). The two main one referred to as the "infrared and big-blue bump" in Calistro Rivera et al. (2016). The peak in the infrared part is due to dust particles in a surrounding dust-torus located outside of the accretion disk, that re-radiates parts of the higher energetic photons from the accretion disk while the other bump in the optical to UV part is created by the primary emission of the accretion disk itself. The issue by assuming black body radiation of a quasar is that one of the bumps is neglected. Doing the same procedure for a star like the Sun, we would consider the whole spectrum to give thermal effects and not neglecting any other additional radiation with longer or shorter wavelengths. In this work the black body fitting is close to the UV-peak to correlate to the wavelengths used in atmospheric models for the Earth-like planets around FGK stars. This means that the possible effects on habitability from the IR range are overlooked. Also the fitted black body spectrum in the optical-UV part creates significantly higher temperatures by a quasar which is outside the interval for where the HZ-models for FGK-stars exist. Therefore the temperatures of the stars is used instead of the quasars. If atmospheric models for the Earth-type planets and more time were available, this stellar temperature could be modulated and as well improve the black-body approximation, since we can look at how the changes will impact the habitability in further ways and in more detail.

5.2 Conical shape

As previously stated the emission was approximated to propagate in the form of a double cone similar to the radio jet. The conical shape is still a valid assumption since the dust torus blocks the radiation to spread near parallel to the accretion plane. However the radio-jet is a more narrow cone than what is limited by the torus. Therefore the opening angle of the cone-shaped emission, referred to as only "jet", to be 15° is an exaggeration and would in

the real case be greater. Increasing this angle gives a shorter kill-radius and becomes equal to the isotropic radiation case when the jet-beams are shaped as two half spheres, i.e when the opening angle reaches $\theta = 180°$, as seen in figure (5.1).
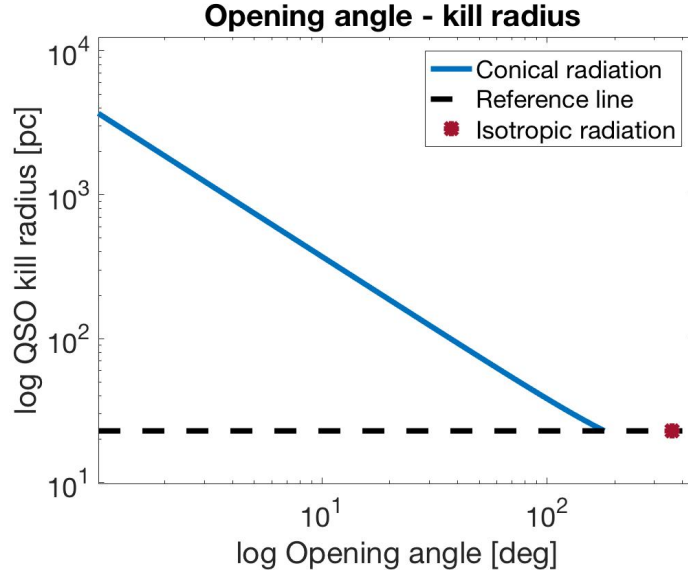

Figure 5.1: *The figure shows the relation between opening angle and kill-radius.*

The change in kill-radius leads to varying mass affected by the QSO radiation as seen in figure (5.2). Therefore when increasing the opening angle, the affected stellar mass decreases and reaches the same impact as from isotropic emission at $\theta = 180°$, similar to previous discussion. The shape of emission, or i.e the opening angle of the jet, is therefore an important factor that needs to be taken into account for this kind of calculations, since the impact of the quasar changes significantly with varying angle.
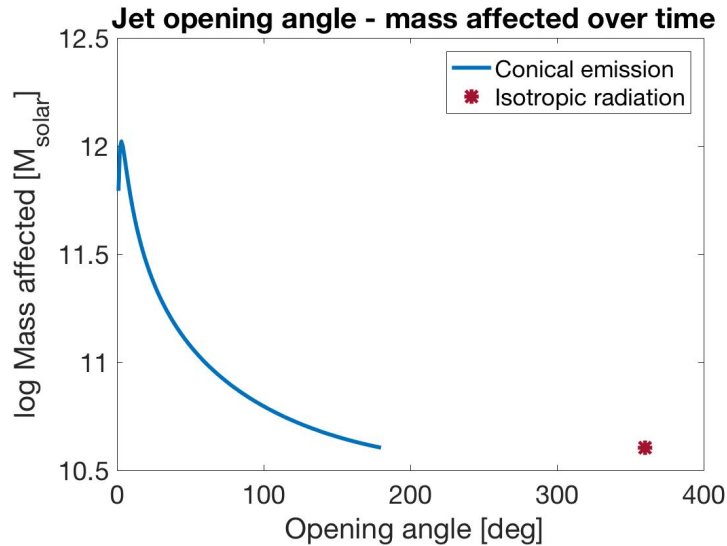

Figure 5.2: *The figure shows how the total stellar mass affected by quasar depends on the opening angle of a jet when stellar movement is considered.*

5.3   Exoplanets

When deriving the number of exoplanets affected by the QSO, we only consider habitable terrestrial planets. These planets are of Earth-type with masses in ranges of 0.5-10$M_\oplus$ including the so-called super-Earths, other types of planets are excluded. In these stellar systems there could also exist other types of life-sustaining planets but the ones considered are the most prominent ones.

Another limitation in this model with a significantly larger impact on the number of exoplanets affected, is that we only consider the FGK-stars. Hence we exclude other stellar systems around stars such as M-dwarfs. These stars are smaller and have a low effective temperature and are the "hot topic" in the latest research for extraterrestrial life. Not only do these types of stars provide a habitable environment on the orbiting planets, but they are also very common. About 90% of the stars in an elliptical galaxy are thought to be M-dwarfs. For this reason, numerous HTPs that do get affected by the thermal radiation is not included in our final result but could be considered in an extension of this project.

5.4   Ideas for future investigations

As a continuation of this thesis there are a few aspects that would be interesting to consider and to improve. One of these is the actual movement of the stars. In order to gain a more accurate result and more realistic stellar movements, it should be encouraged to simulate the movements by e.g an N-body simulation to get statistics like the number of passing stars through the jet, in order to improve the accuracy of the quasar effects. This lies outside the scope of this thesis and its time restrictions but would definitely be an improvement to the model applied here.

As a second aspect, one could also consider other effects from the quasar radiation in other wavelengths as an addition to the effects by the considered range in this thesis. As previously mentioned the SED consists of two bumps and only one was taken into account. The addition of ionization effects is likely to enhance the radiation effects that could imply a kill-radius that extends further out in the galaxy and so a higher amount of affected stellar systems.

Chapter 6

Conclusion

In this thesis we have investigated the influence of a quasar on the habitability in its host galaxy, namely by the thermal effects it brings to the habitable terrestrial planets. By adapting a model of the habitable zone around a star, the inner limit of the HZ of the quasar was equated to the kill-radius. Together with other assumptions and pre-existing equations, we were able to estimate the number of HTPs that sometime in galactic history has been exposed to potentially lethal radiation from a quasar. The number of exoplanets affected in the galaxies with stellar masses 10^9 $M_\odot$, 10^{10} $M_\odot$ and 10^{13} $M_\odot$ were estimated to 1×10^6, 8×10^6 and 3×10^9 for a double-conical shaped emission from the quasar. The result can also be expressed as a fraction of stellar mass affected over total stellar mass in the galaxy, 12.8%, 9.5% and 3.8%. Based on the result we can conclude that the quasar might not be the "destroyer of worlds" we were hoping for, if only thermal effects are considered. Additionally given the assumptions made, the result is most likely an upper limit which then reduces the impacts even more in the real case. While the fraction of exoplanets affected by the quasar within its host galaxy is consistently predicted to be small ($\sim 10\%$ at the most), the absolute number of affected exoplanets may be a few billions for the most massive galaxies.

We can rule out the importance of temperature considering this model and emphasize the importance of stellar movement and time of quasar activity along with the significant dependence of directional emission such as the jet-beam shaped emission. To improve the calculations a simulation of the stellar movement in an elliptical galaxy is the key factor. Getting a more accurate situation of the movement of the stars would give an even more realistic result. To extend the research, one could include the other effects from a quasar, that are likely to provide a greater number of planets affected and giving back the quasar its reputation as a destroyer of worlds.

Acknowledgement

Bibliography

Akritas, M. G. & Bershady, M. A. (1996), 'Linear Regression for Astronomical Data with Measurement Errors and Intrinsic Scatter', *The Astrophysical Journal* **470**, 706.

Antonucci, R. (1993), 'Unified models for active galactic nuclei and quasars', *Annual Review of Astronomy Astrophysics* **31**, 473–521.

Balbi, A. & Tombesi, F. (2017), 'The habitability of the Milky Way during the active phase of its central supermassive black hole', *Scientific Reports* **7**, 16626.

Calistro Rivera, G., Lusso, E., Hennawi, J. F. & Hogg, D. W. (2016), 'AGNfitter: A Bayesian MCMC Approach to Fitting Spectral Energy Distributions of AGNs', *The Astrophysical Journal* **833**, 98.

Clarke, J. N. (1981), 'Extraterrestrial intelligence and galactic nuclear activity', *Icarus* **46**, 94–96.

Cuntz, M. (2014), 'S-type and P-type Habitability in Stellar Binary Systems: A Comprehensive Approach. I. Method and Applications', *The Astrophysical Journal* **780**, 14.

Elvis, M., Hao, H., Civano, F., Brusa, M., Salvato, M., Bongiorno, A., Capak, P., Zamorani, G., Comastri, A., Jahnke, K., Lusso, E., Mainieri, V., Trump, J. R., Ho, L. C., Aussel, H., Cappelluti, N., Cisternas, M., Frayer, D., Gilli, R., Hasinger, G., Huchra, J. P., Impey, C. D., Koekemoer, A. M., Lanzuisi, G., Le Floc'h, E., Lilly, S. J., Liu, Y., McCarthy, P., McCracken, H. J., Merloni, A., Roeser, H.-J., Sanders, D. B., Sargent, M., Scoville, N., Schinnerer, E., Schiminovich, D., Silverman, J., Taniguchi, Y., Vignali, C., Urry, C. M., Zamojski, M. A. & Zatloukal, M. (2012), 'Spectral Energy Distributions of Type 1 Active Galactic Nuclei in the COSMOS Survey. I. The XMM-COSMOS Sample', *The Astrophysical Journal* **759**, 6.

Forbes, J. C. & Loeb, A. (2018), 'Evaporation of planetary atmospheres due to XUV illumination by quasars', *Monthly Notices of the Royal Astronomical Society* **479**, 171–182.

Gale, J. & Wandel, A. (2017), 'The potential of planets orbiting red dwarf stars to support oxygenic photosynthesis and complex life', *International Journal of Astrobiology* **16**, 1–9.

Habets, G. M. H. J. & Heintze, J. R. W. (1981), 'Empirical bolometric corrections for the main-sequence', *Astronomy Astrophysics, Supplement* **46**, 193–237.

Häring, N. & Rix, H.-W. (2004), 'On the Black Hole Mass-Bulge Mass Relation', *The Astrophysical Journal , Letters* **604**, L89–L92.

Kasting, J. F., Kopparapu, R., Ramirez, R. M. & Harman, C. E. (2014), 'Remote life-detection criteria, habitable zone boundaries, and the frequency of Earth-like planets around M and late K stars', *Proceedings of the National Academy of Science* **111**, 12641–12646.

Kasting, J. F., Whitmire, D. P. & Reynolds, R. T. (1993), 'Habitable Zones around Main Sequence Stars', *Icarus* **101**, 108–128.

King, A. (2016), 'How big can a black hole grow?', *Monthly Notices of the Royal Astronomical Society* **456**, L109–L112.

King, A. & Pounds, K. (2015), 'Powerful Outflows and Feedback from Active Galactic Nuclei', *Annual Review of Astronomy Astrophysics* **53**, 115–154.

Lacis, A. A. & Hansen, J. (1974), 'A parameterization for the absorption of solar radiation in the earth's atmosphere', *Journal of the Atmospheric Sciences* **31**(1), 118–133.

Lingam, M., Ginsburg, I. & Bialy, S. (2019), 'Active Galactic Nuclei: Boon or Bane for Biota?', *arXiv e-prints* .

Martini, P. (2004), 'QSO Lifetimes', *Coevolution of Black Holes and Galaxies* p. 169.

Meier, D. L. (2012), *Black Hole Astrophysics*, Springer, Berlin, Heidelberg.

Melott, A. L. & Thomas, B. C. (2011), 'Astrophysical Ionizing Radiation and Earth: A Brief Review and Census of Intermittent Intense Sources', *Astrobiology* **11**, 343–361.

Munari, E., Biviano, A., Borgani, S., Murante, G. & Fabjan, D. (2013), 'The relation between velocity dispersion and mass in simulated clusters of galaxies: dependence on the tracer and the baryonic physics', *Monthly Notices of the Royal Astronomical Society* **430**, 2638–2649.

Plummer, H. C. (1911), 'On the problem of distribution in globular star clusters', *Monthly Notices of the Royal Astronomical Society* **71**, 460–470.

Pushkarev, A. B., Kovalev, Y. Y., Lister, M. L. & Savolainen, T. (2011), 'Opening angles of parsec-scale AGN jets', *Memorie della Società Astronomica Italiana* **82**, 190.

Selsis, F., Kasting, J. F., Levrard, B., Paillet, J., Ribas, I. & Delfosse, X. (2007), 'Habitable planets around the star Gliese 581?', *Astronomy Astrophysics* **476**, 1373–1387.

Shankar, F., Crocce, M., Miralda-Escudé, J., Fosalba, P. & Weinberg, D. H. (2010), 'On the Radiative Efficiencies, Eddington Ratios, and Duty Cycles of Luminous High-redshift Quasars', *The Astrophysical Journal* **718**, 231–250.

Stanway, E. R., Hoskin, M. J., Lane, M. A., Brown, G. C., Childs, H. J. T., Greis, S. M. L. & Levan, A. J. (2018), 'Exploring the cosmic evolution of habitability with galaxy merger trees', *Monthly Notices of the Royal Astronomical Society* **475**, 1829–1842.

Zackrisson, E., Calissendorff, P., González, J., Benson, A., Johansen, A. & Janson, M. (2016), 'Terrestrial Planets across Space and Time', *The Astrophysical Journal* **833**, 214.

Chapter 7

Appendix

The matlab code providing all mentioned calculations.

7.0.1   Main Matlab code

```matlab
%% Mass , bulge -SMBH -Bolometric luminosity

m_b_sol =10.^[9 10 13];                          %solarmass
lg_m_BH_sol = 8.2 + 1.12* log10 (m_b_sol/(1e11)); %solarmass ,
    mass of black hole log

m_BH_sol =10.^ lg_m_BH_sol;                       %solarmass ,
    mass of black hole log

L_edd_ergs =(1.26*10^38).* m_BH_sol;              % [ergs^-1], 1
    erg =10^-7J , Eddington luminosity
L_edd_sol=L_edd_ergs./(3.828*10^33);             %Eddington
    luminosity [solar unit ]

L_bol_ergs=L_edd_ergs *0.1;                       % Luminosity
    10% of Eddington luminosity [ergs^-1]


%% Gets the QSO spectrum and calculates the luminosity for the
    whole spectrum and the limited range
%Range: 1000-40 000 [  ] i.e 2.9979e15 -7.4948e+13 [Hz]

%Selsis constants
l_ins =0.84;          %[AU]   chosen from table 2 from Cuntz 1,
    runway greenhouse , max greenhouse no clouds
a_in =2.7619*10^-5;  %[AU]
b_in =3.8095*10^-9;  %[AU]

% http://www.graphreader.com/
%Fig.14 H Elvis (2012) mean SED radio quiet
%x=log(v) [Hz]    fig 6 i restframe
%y=v*L [ergs^-1] fig 6
log_freq_Hz
    =[9.679,9.737,9.763,9.867,10.074,10.281,10.332,10.423,10.604,10.824,...
```

```matlab
    11.16 ,11.419 ,11.678 ,11.911 ,12.157 ,12.364 ,12.532 ,12.7 ,12.984 ,13.243 ,...

    13.398 ,13.67 ,13.942 ,14.123 ,14.226 ,14.382 ,14.589 ,14.757 ,14.886 ,15.003 ,...

    15.158 ,15.339 ,15.572 ,15.727 ,16.025 ,16.219 ,16.464 ,16.658 ,16.878 ,17.215 ,...

    17.473 ,17.68 ,17.849 ,17.978 ,18.224 ,18.34 ,18.457 ,18.573 ,18.741 ,18.942];


log_Lv_ergs
    =[38.31 ,39.047 ,39.641 ,39.718 ,39.731 ,39.77 ,40.003 ,40.287 ,40.674 ,41.127 ,...

    41.76 ,42.276 ,42.78 ,43.284 ,43.788 ,44.176 ,44.563 ,44.848 ,45.132 ,45.3 ,...

    45.377 ,45.3 ,45.3 ,45.274 ,45.132 ,45.028 ,45.08 ,45.196 ,45.351 ,45.494 ,...

    45.597 ,45.623 ,45.532 ,45.364 ,45.209 ,45.016 ,44.886 ,44.705 ,44.576 ,...

    44.576 ,44.576 ,44.576 ,44.525 ,44.641 ,44.705 ,44.705 ,44.512 ,44.357 ,...

    44.279 ,44.266];

Lv_ergs =10.^ log_Lv_ergs; %[ergs^-1]
freq_tot_Hz =10.^ log_freq_Hz;% [Hz]

% KGF -Star
T_eff =5800; %[K] solar temperature approx
T_sun =5700;
T=T_eff - T_sun ;

% Quasar luminosity
%picks the limited wavelength range
freq_Hz=freq_tot_Hz (23:32); %the frequencies in the range we
    want [Hz]
lum_freq_range_ergs=Lv_ergs (23:32);    %corresponding "
    luminosity" vector in the wanted range [ergs^-1]

x_range_Hz =[];                  % Empty vector for stepsize [Hz]
for i= 1:length(freq_Hz) -1   % Nr of  iterationes = lenght(freq
    )-1
    j=i+1;                   % picks next value in vector
diff=freq_Hz(j)-freq_Hz(i);     % calc. step size in frequency
x_range_Hz(j)=diff;          %Saves step size in vector
end

L_SED_ergs_Hz=lum_freq_range_ergs ./freq_Hz;        %[erg*s^-1*Hz
    ^-1]
lumos_SED_ergs=trapz (x_range_Hz ,L_SED_ergs_Hz );   % L [erg*s
    ^-1]

x_range_bol_Hz =[];
for i= 1:length(freq_tot_Hz) -1
    j=i+1;
diff_bol=freq_tot_Hz(j)-freq_tot_Hz(i);
x_range_bol_Hz(j)=diff_bol;
```

```matlab
end

L_bol_SED_ergs_Hz=Lv_ergs./freq_tot_Hz;                    %[
    erg*s^-1*Hz^-1]
lumos_bol_SED_ergs=trapz(x_range_bol_Hz,L_bol_SED_ergs_Hz); % [
    ergs^-1]
L_ratio=lumos_SED_ergs/lumos_bol_SED_ergs;


L_ergs = L_ratio*L_bol_ergs; % ratio between the whole spectra
    and limited range * bolometric luminosity from mass-relation

%% Jet shaped emission

theta=15*pi/180; %rad 15
solid_angle_cone=2*pi*(1-cos(theta/2)); %sterr.
R_angle=4*pi/(2*solid_angle_cone);
L_jet=L_ergs*R_angle;


%% Equations for kill radius
d_kill_pc=((l_ins-a_in.*T-b_in.*T.^2).*sqrt(L_jet/(3.828*10^33)
    ))/206265;
d_kill_pc_spherical = ((l_ins-a_in.*T-b_in.*T.^2).*sqrt(L_ergs
    /(3.828*10^33)))/206265;

d_rough_kill=[];
for i=1:3
d_rough_kill(i)=sqrt(L_bol_ergs(i)/(3.828*10^33))/206265; %[pc]
end


%% Mass inside killradous
a=48.*sqrt(m_b_sol/(1e10)); %pc

f1= @(r1) 3*m_b_sol(1)*a(1)^2./(4*pi.*(a(1)^2+r1.^2).^(5/2))*2*
    pi*(1-cos(theta/2)).*r1.^2;  % m_b_sol i solenhet
mass_sol(1)=2*integral(f1,0,d_kill_pc(1));

f2= @(r2) 3*m_b_sol(2)*a(2)^2./(4*pi.*(a(2)^2+r2.^2).^(5/2))*2*
    pi*(1-cos(theta/2)).*r2.^2;  % m_b_sol i solenhet
mass_sol(2)=2*integral(f2,0,d_kill_pc(2));

f3= @(r3) 3*m_b_sol(3)*a(3)^2./(4*pi.*(a(3)^2+r3.^2).^(5/2))*2*
    pi*(1-cos(theta/2)).*r3.^2;  % m_b_sol i solenhet
mass_sol(3)=2*integral(f3,0,d_kill_pc(3));

%% for spherical case
f1_s= @(r1_s) 3*a(1)^2*m_b_sol(1)*r1_s.^2./((r1_s.^2+a(1)^2)
    .^(5/2));  % m_b_sol i solenhet
mass_sol_spherical(1)=integral(f1_s,0,d_kill_pc_spherical(1));


f2_s= @(r2_s) 3*a(2)^2*m_b_sol(2)*r2_s.^2./((r2_s.^2+a(2)^2)
    .^(5/2));
```

```matlab
mass_sol_spherical(2)=integral(f2_s,0,d_kill_pc_spherical(2));


f3_s= @(r3_s) 3*a(3)^2*m_b_sol(3)*r3_s.^2./((r3_s.^2+a(3)^2)
    .^(5/2));
mass_sol_spherical(3)=integral(f3_s,0,d_kill_pc_spherical(3));

%% M-sigma relation
sigma_km_s=(m_b_sol./1e10).^(1/4)*108; % [kms^-1]   from book
    with core rad.
sigma_pc_yrs=sigma_km_s*3.2407792896664e-14*(60*60*24*365.25)/
    sqrt(3); % [pc]        SQRT(3) PGA 1D

t_QSO=1e8; %[yrs] try for 1e6, 1e7 & 1e8

%jet
for i=1:3
MFR=@(r_test) sigma_pc_yrs(i).*t_QSO*theta*r_test*a(i).^2.*
    m_b_sol(i)*3./(4*pi*(a(i).^2+r_test.^2).^(5/2)); %mass flow
    rate over time
tot_mass_during_time(i)=2*integral(MFR,0,d_kill_pc(i));

if i==1
tot_mass_during_time(1)=tot_mass_during_time(i);
end

if i==2
tot_mass_during_time(2)=tot_mass_during_time(i);
end

if i==3
tot_mass_during_time(3)=tot_mass_during_time(i);
end

end

%%
%sphere
for i=1:3
MFR=@(r_test) sigma_pc_yrs(i).*t_QSO*a(i).^2.*m_b_sol(i)*3./(4*
    pi*(a(i).^2+d_kill_pc_spherical(i).^2).^(5/2))*2*pi*r_test;
    %mass flow rate over time
tot_mass_during_time_spherical(i)=integral(MFR,0,
    d_kill_pc_spherical(i));

if i==1
tot_mass_during_time_spherical(1)=
    tot_mass_during_time_spherical(i);
end

if i==2
tot_mass_during_time_spherical(2)=
    tot_mass_during_time_spherical(i);
end
```

```matlab
if i==3
tot_mass_during_time_spherical(3)=
    tot_mass_during_time_spherical(i);
end

end

total_mass_during_time_spherical=tot_mass_during_time_spherical
    ;

%% Fraction & Nr of stars affected

Frac_affected_stars= tot_mass_during_time./m_b_sol;

Frac_affected_stars_spherical= total_mass_during_time_spherical
    ./m_b_sol;

%% Exoplanets

Nr_planets=tot_mass_during_time*0.035/4;
Nr_planets_spherical=total_mass_during_time_spherical*0.035/4;
%%Erik et al. 2016  https://iopscience.iop.org/article
    /10.3847/1538-4357/833/2/214/pdf


%%
disp('(1)= Small ellipse (2)= Bulge (3)=Large ellipse')
disp(' ')
disp(['log-Bolometric luminosity: ' num2str(log10(L_bol_ergs))
    '[ergs^-1]'])
disp(['log-Luminosity in limited range: ' num2str(log10(L_ergs)
    ) '[ergs^-1]'])
disp(sprintf( ' log -Mass of black hole [Msol]: %d, %d, %d',
    m_BH_sol))
disp(sprintf('Core radius [pc]: %d, %d %d', a))
disp(['Rough estimate of QSO kill radius, w/ L_bol: ' num2str(
    d_rough_kill) '[Pc]' ])
disp(' ')

disp('Spherical case')
disp(['QSO kill radius for spherical rad.: ' num2str(
    d_kill_pc_spherical) '[pc]'])
disp(sprintf( 'Mass inside kill radius moment. [Msol]: %d, %d,
    %d',mass_sol_spherical ))
disp(sprintf( 'Mass inside kill radius over time, [Msol]: %d, %
    d, %d',total_mass_during_time_spherical ))
disp([ 'Frac. stellar mass over time: ' num2str(
    Frac_affected_stars_spherical*100) '[%]' ])
disp(sprintf( 'Number of affected exoplanets: %d, %d, %d' ,
    Nr_planets_spherical))
disp(' ')

disp('Jet case')
disp([ 'QSO kill radius for jet: ' num2str(d_kill_pc) '[Pc]'])
```

```matlab
disp(sprintf( 'Mass inside kill radius moment. [Msol]: %d, %d,
    %d', mass_sol))
disp(sprintf( 'Mass inside kill radius over time [Msol]: %d, %d
    , %d' ,tot_mass_during_time ))
disp([ 'Frac.stellar mass over time: ' num2str(
    Frac_affected_stars*100) '[%]' ])
disp(sprintf( 'Number of affected exoplanets: %d, %d, %d' ,
    Nr_planets))

%% Get half mass radius

%1
r=1;
half_mass=1;

while half_mass<(m_b_sol(1)/2)
    r=r+1;
vol_dens= @(r) a(1).^2.*m_b_sol(1)*3.*r.^2./((a(1).^2+r.^2)
    .^(5/2));
half_mass= integral(vol_dens,0,r);
end
disp(['r= ' num2str(r)])

%2
r_2=1;

while half_mass<(m_b_sol(2)/2)
    r_2=r_2+1;
vol_dens2= @(r_2) a(2).^2.*m_b_sol(2)*3.*r_2.^2./((a(2).^2+r_2
    .^2).^(5/2));
half_mass= integral(vol_dens2,0,r_2);
end
disp(['r= ' num2str(r_2)])

%3
r_3=1;

while half_mass<(m_b_sol(3)/2)
    r_3=r_3+1;
vol_dens3= @(r_3) a(3).^2.*m_b_sol(3)*3.*r_3.^2./((a(3).^2+r_3
    .^2).^(5/2));
half_mass= integral(vol_dens3,0,r_3);
end
disp(['r= ' num2str(r_3)])

r_vec=[r r_2 r_3];

%% Plots and figures
% Plot spherical vs conical for relation between killradius and
    bulge mass
figure(1)
figure_1=plot(log10(m_b_sol),log10(d_kill_pc),'-r',log10(
    m_b_sol),log10(d_kill_pc_spherical),'-b',log10(m_b_sol),
    log10(a),'-m',log10(m_b_sol),log10(r_vec),'-',log10(m_b_sol)
    ,log10(d_rough_kill),'-',log10(m_b_sol),log10(d_kill_pc),'*r
```

```matlab
       ',log10(m_b_sol),log10(d_kill_pc_spherical),'*b');
title('\bf Bulge mass - Kill radius relation')
xlabel(' log Bulge mass [M_{solar}]')
ylabel(' log QSO Kill radius [pc]')
legend('Jet radiation','Isotropic radiation','Core radius','
    half-mass radius','Rough estim. ')
set(gca,'FontSize',20)
set(figure_1,'LineWidth',3,'MarkerSize',10)

%%
%jet
for j=1:180
theta(j)=j*pi/180;

    solid_angle_cone_vec(j)=2*pi*(1-cos(theta(j)/2)); %sterr.
    L_jet_vec(j)=L_ergs(3)*4*pi./(2*solid_angle_cone_vec(j));
    d_kill_pc_vec(j)=((l_ins-a_in.*T-b_in.*T.^2).*sqrt(
        L_jet_vec(j)/(3.828*10^33)))/206265;

MFR=@(r_test) sigma_pc_yrs(3).*t_QSO*theta(j)*r_test*a(3).^2.*
    m_b_sol(3)*3./(4*pi*(a(3).^2+r_test.^2).^(5/2)); %mass flow
    rate over time
tot_mass_during_time_vec(j)=2*integral(MFR,0,d_kill_pc_vec(j));

j=j+1;
end

%Over time
figure(3) % for large ellipse
figure_3=plot(theta*180/pi,log10(tot_mass_during_time_vec),'-b'
    ,360,log10(total_mass_during_time_spherical(3)),'*r');
title('\bf Jet opening angle - mass affected over time')
xlabel(' Opening angle [deg]')
ylabel('log Mass affected [M_{solar}]')
legend('Conical emission','Isotropic radiation')
set(gca,'FontSize',20)
set(figure_3,'LineWidth',3,'MarkerSize',10)

% plot the SED
log10_freq_tot_Hz=log10(freq_tot_Hz);
log10_Lv_ergs=log10(Lv_ergs);
log10_freq_Hz=log10(freq_Hz);
log10_lum_freq_range_ergs=log10(lum_freq_range_ergs);
y_limit_for_transparancy = zeros(10, 1);
y_limit_for_transparancy(:) = 50;
figure(4)
H=area(log10_freq_Hz,y_limit_for_transparancy);
set(H,'FaceColor',[0.70 0.15 0.10]);
set(H,'facealpha',0.99)
hold on
figure_4=plot(log10_freq_tot_Hz,log10_Lv_ergs,'-k');
title('\bf SED of quasar')
xlabel(' log \nu    [ Hz ]')
ylabel(' log L  [ erg s^{-1} Hz^{-1}) ] ')
legend('Examined frequency range ','Total luminosity')
```

```
set(gca,'FontSize',24)
set(figure_4,'LineWidth',3)
axis([9 19 39 46])

% Plot bulge mass-black hole relation
figure(5)
figure_5=plot(log10(m_b_sol),log10(m_BH_sol),'k-',log10(m_b_sol
    (1)),log10(m_BH_sol(1)),'b*',log10(m_b_sol(2)),log10(
    m_BH_sol(2)),'r*',log10(m_b_sol(3)),log10(m_BH_sol(3)),'m*')
    ;
xlabel(' log M_b [  M_{solar} ]')
ylabel(' log M_{BH} [  M_{solar} ] ')
title('\bf Bulge - Black hole mass relation')
legend(' ', 'bulge mass 10^{9}', 'bulge mass 10^{10} ', 'bulge
    mass 10^{13}')
set(gca,'FontSize',20)
set(figure_5,'LineWidth',3,'MarkerSize',10)

%% Opening angle - kill radius
line_for_90_deg=zeros(400, 1);
line_for_90_deg(:)=d_kill_pc_spherical(3);
theta_vec_long=(1:1:400)*pi/180;

figure(6)
figure_6=loglog(theta*180/pi,d_kill_pc_vec,'-',theta_vec_long
    *180/pi,line_for_90_deg,'--',360,d_kill_pc_spherical(3),'*')
    ;
xlabel('log Opening angle [deg]')
ylabel('log QSO kill radius [pc]')
legend('Conical radiation','Reference line','Isotropic
    radiation')
title('Opening angle - kill radius ')
set(gca,'FontSize',20)
set(figure_6,'LineWidth',4,'MarkerSize',10)
```

7.0.2 Temperature independence

```
% Constants from (Cuntz 2013), tabel 2
a_in=2.7619*10^-5;%[AU]
b_in=3.8095*10^-9;
a_out=1.3786*10^-4;
b_out=1.4286*10^-9;

l_ins=0.84;%[AU]  runway greenhouse
l_outs= 1.67;% max greenhouse no clouds

T_eff=3900:100:7600;
T_sun=5700;
T=T_eff-T_sun;%[K]

L=3.828*10^33; %[ergs^-1] solar luminosity

d_in=((l_ins-a_in.*T-b_in.*T.^2).*sqrt(L/(3.828*10^33))); %[AU]
    Selsis methode
d_out=((l_outs-a_out.*T-b_out.*T.^2).*sqrt(L/(3.828*10^33))); %
```

```
    [AU] Selsis methode


figure(1)
figure1=plot(d_in,T_eff,'-b',d_out,T_eff,'-r');
legend('Inner limit for HZ', 'Outer limit for HZ')
xlabel('Distance from star [AU]')
ylabel('T_{eff} [K]')
title('\bf Limits for Habitable Zone with Selsis method')
grid on
set(gca,'FontSize',20)
set(figure1,'LineWidth',4)
```

7.0.3 Stellar mass and black hole mass relations

```
m_b_sol=10.^(8:1:14); %Bulge mass (8.36) from Mendel et al 2013
lg_m_BH_sol = 8.2 + 1.12*log10(m_b_sol/(1e11)); %[solarunit],
    mass of black hole log

m_BH_sol=10.^lg_m_BH_sol; %[solarunit], mass black hole

L_edd_ergs=(1.26*10^38).*m_BH_sol; % [ergs^-1], 1erg=10^-7J ,
    Eddington luminosity
L_edd_sol=L_edd_ergs./(3.828*10^33); %Eddington luminosity [
    solarunit]

L_bol_ergs=L_edd_ergs*0.1; % Luminosity 10% of Eddington
    luminosity [ergs^-1]
L=L_bol_ergs*0.35048;

figure(1)
plot(m_b_sol,L_bol_ergs,'-')
xlabel('mass of bulge [solar unit]')
ylabel('Luminosity of AGN [ergs^-1]')
title('Bulgemass - Luminosity relation')
solar=char(9737);

figure(3)
plot(m_BH_sol,L_bol_ergs,'*')
xlabel('Black hole mass [solar unit]')
ylabel('Luminosity [ergs^-1] 10% of eddington ')
title('Luminosity - Black hole mass relation')

figure(2)
figure_2=plot(log10(m_b_sol),log10(m_BH_sol),'k-',log10(m_b_sol
    (2)),log10(m_BH_sol(2)),'*',log10(m_b_sol(3)),log10(m_BH_sol
    (3)),'*',log10(m_b_sol(6)),log10(m_BH_sol(6)),'*')
xlabel('logM_b [  M_{solar} ]')
ylabel('logM_{BH} [  M_{solar} ] ')
title('Bulge - Black hole mass relation')
legend(' ', 'bulge mass 10^{9}', 'bulge mass 10^{10} ', 'bulge
    mass 10^{13}')
set(gca,'FontSize',22)
set(figure_2,'LineWidth',3,'MarkerSize',10)
```